

## Article

# Variable-Speed Frequency-Hopping Signal Sorting: Spectrogram Is Sufficient

Weipeng Zhu <sup>1</sup>, Hu Jin <sup>1</sup>, Jin Wang <sup>1</sup>, Yingke Lei <sup>1</sup>, Caiyi Lou <sup>2,\*</sup> and Changming Liu <sup>3</sup>

<sup>1</sup> College of Electronic Engineering, National University of Defense Technology, Hefei 230037, China; m13357188541@163.com (W.Z.); zhangzhi@nudt.edu.cn (H.J.); ww2907545@163.com (J.W.); leiyingke@163.com (Y.L.)

<sup>2</sup> Jiaxing Communication Information Security Control Laboratory Technology Research Institute, The 36th Research Institute of China Electronics Technology Group Corporation, Jiaxing 314033, China

<sup>3</sup> Tong Fang Electronic Science Technology Co., Ltd., Jiujiang 332005, China; mrlcm@126.com

\* Correspondence: loucai@126.com

**Abstract:** In this paper, we present a novel signal sorting method aimed at reducing the impact of interference and noise while achieving blind detection and accurate sorting of a variable-speed frequency-hopping communication system. To achieve this, we combine spectrogram analysis with an innovative sorting approach. First, we generate the spectrogram of the received signal, and then employ a morphology filter to effectively eliminate noise and sweep frequency interference from the spectrogram. Subsequently, we identify and mark connected domains in the spectrogram, from which we extract the duration data to create a dataset specifically for separating fixed-frequency interference. Furthermore, we propose a specialized time alignment algorithm designed to accommodate the unique characteristics of variable-speed frequency-hopping signals, enabling precise sorting of variable-speed frequency-hopping signals. Through rigorous comparative evaluations against existing algorithms, we demonstrate that our proposed approach provides superior accuracy by offering a clearer representation of the time–frequency situation of the received signals. The proposed method provides a high correct sorting probability which is equal to 0.8 when signal-to-noise ratio is 0 dB and reaches 1 when signal-to-noise ratio reaches over 12 dB. In comparison, the correct sorting probability of the comparison algorithm is far inferior to the proposed algorithm.



**Citation:** Zhu, W.; Jin, H.; Wang, J.; Lei, Y.; Lou, C.; Liu, C. Variable-Speed Frequency-Hopping Signal Sorting: Spectrogram Is Sufficient. *Electronics* **2023**, *12*, 4533. <https://doi.org/10.3390/electronics12214533>

Academic Editor: Esteban Telo-Cuautle

Received: 16 August 2023  
Revised: 27 September 2023  
Accepted: 30 September 2023  
Published: 3 November 2023



**Copyright:** © 2023 by the authors. Licensee MDPI, Basel, Switzerland. This article is an open access article distributed under the terms and conditions of the Creative Commons Attribution (CC BY) license (<https://creativecommons.org/licenses/by/4.0/>).

**Keywords:** variable-speed frequency-hopping signals; signal sorting; spectrogram; time alignment

## 1. Introduction

Frequency-hopping (FH) communication, as a special spread spectrum communication method, can randomly change the carrier frequency of the signal according to a certain pattern, and has superior antifading, anti-interference, and anti-interception capabilities. With the widespread application of FH communication technology in the military field, there have been increasing demands for reconnaissance of FH signals from noncooperative parties.

The sorting of FH signals is a fundamental problem in the reconnaissance of FH signals [1]; extensive studies have been devoted to this area and many methods have been proposed to precisely sort FH signals from multiple networks. The multiple-hop autocorrelation processing is considered a traditional means of estimating the parameters and sorting the networks of FH signals in the presence of broadband thermal noise, which is dependent on prior information [2]. In [3], a shortwave signal detection algorithm based on spectral energy statistics was proposed, utilizing the differences in the energy spectrum characteristics of shortwave signals. However, the detection probability was poor at low signal-to-noise ratios (SNRs). In [4], the authors proposed a channelized structure based on short-time Fourier transform (STFT), which was only based on signal power detection, but the detection effect plummeted at low SNR. In [5], autocorrelation processing was

performed on each subchannel signal to achieve FH signal detection after channelization processing of the received signal. Once the FH signal crosses the channel, a certain hop of the FH signal is lost, resulting in a decrease in detection probability. In [6], the authors generated time–frequency maps using an overlapping sliding window to improve time–frequency resolution and signal detection probability. In [7], the authors used the method of short-term energy cancellation to detect the existence of FH signals in each subchannel, while ignoring the cross-channel problem of FH signals. In [8], local adaptive thresholds were set to eliminate the impact of interference signals, but the detection probability and anti-interference ability are poor in shortwave channels.

FH signal sorting essentially belongs to the classification problem; as a result, many clustering algorithms are applied to that. Both FH threshold segmentation algorithm based on the K-means [9] and feature set classification algorithm based on the improved K-Means [10] can extract FH signals at low SNR, with high detection probabilities. However, the K-means clustering algorithm requires presetting of the number of clusters and has weak anti-interference ability in shortwave channels.

In recent years, deep learning has emerged in the field of FH signal sorting. In [11–13], the impact of spectrum leakage and poor time–frequency resolution was reduced to improve detection probability through the method of neural network. The real electromagnetic environment is complex and unpredictable, which poses a problem to the detection algorithm based on simulation data. To address this problem, an interference cancellation network that introduces a graph attention mechanism and an ensemble channel attention module with Siamese nested U-Net backbone was proposed [14], but requires a great lot of calculation.

Because of technical performance and computation limitations, it is more universal to use time–frequency spectrum information to sort signals in engineering. In [15], the utilization of smooth pseudo-Wigner–Ville distribution (SPWVD) to generate time–frequency maps increased the computational complexity and was not conducive to engineering implementation. The time–frequency maps were obtained through STFT, and then processed using image enhancement, edge detection, and morphological filtering methods [16,17]. This had a good effect on interference with geometric features. To solve the problem of selection of structural elements in traditional methods, a morphological structure adaptive method was proposed, which combines with the least squares method to improve the estimation accuracy [18].

Due to the rapid development of FH communication, multiple types of FH communication technologies have emerged, and variable-speed FH communication technology stands out among them, which adopts the strategy of variable FH speed to pose a severe challenge on the sorting of FH signals in complex environments [19]. Some scholars have proposed blind source separation algorithm, sparse Bayesian estimation algorithm, and frame overlap algorithm to sort variable-speed FH signals from different receiving time periods [20–25]. However, the practical application of these algorithms are limited by their large computational complexity and poor sorting accuracy.

Motivated by the study in [16], we consider a sorting method for variable-speed FH signals with only a spectrogram. Our focus is to detect the variable-speed FH signals from complex electromagnetic environments and separate the multiple variable-speed FH signals into the single variable-speed FH signal corresponding to the same radio station with only a spectrogram. Results indicate that the proposed method can accurately select variable-speed FH signals with the good antinoise ability and anti-interference ability. Our work contributes in the following aspects:

- This method does not require preprocessing of the received signal and only requires obtaining the spectrogram of the received signal, which reduces computational complexity.
- We repair the broken part of the spectrogram which is caused by the noise and interference to offer better representation of the time–frequency situation.
- We develop the time alignment algorithm for the characteristics of variable-speed FH signal, and this algorithm improves sorting accuracy significantly.

The remainder of this paper is organized as follows. In Section 2, the mathematical model of signal and time–frequency analysis are introduced. In Section 3, the proposed algorithm for variable-speed FH signal sorting is presented. The output result and sorting accuracy of the proposed algorithm are numerically evaluated in Section 4, and conclusions are made in Section 5.

## 2. Signal Model and Problem Formulation

### 2.1. Signal Model

We assume that there are noise, fixed-frequency interference, and sweep-frequency interference in the shortwave environment. Within the certain observation time, we can model the received signal in the shortwave frequency channel by

$$r(t) = \sum_{i=1}^I FSFH_i(t) + \sum_{j=1}^J VSFH_j(t) + \sum_{k=1}^K d_k(t) + \sum_{l=1}^L c_l(t) + n(t) \quad (1)$$

where  $r(t)$  is the received shortwave broadband signal,  $FSFH(t)$  is the fixed-speed FH signal,  $VSFH(t)$  is the variable-speed FH signal,  $d(t)$  is the fixed-frequency interference,  $c(t)$  is the sweep-frequency interference, and  $n(t)$  is the receiver noise (we assume that it is white and Gaussian).

Assume that the period of the fixed-speed FH signal is  $T_h$  and the amplitude of the fixed-speed FH signal is  $A(t)$ . To describe the FH signal, we introduce the rectangular window function, which can be written as

$$\text{rect}_{T_h}(t) = \begin{cases} 1 & 0 \leq t \leq T_h \\ 0 & \text{else} \end{cases} \quad (2)$$

According to reference [26], the model of the fixed-speed FH signal can be given by

$$FSFH(t) = A(t) * \sum_n \text{rect}_{T_h}(t - (n-1)T_h - t_0) e^{j2\pi f_n(t - (n-1)T_h - t_0) + j\theta_n} * m(t) \quad (3)$$

where  $t_0$  is the original time,  $f_n$  is the center frequency at hop  $n$ ,  $\theta_n$  is the initial phase at hop  $n$ , and  $m(t)$  denotes an information modulation term multiplied to the FH signal.

Compared with the fixed-speed FH signal, the period of the variable-speed FH signal changes randomly. Based on (3), the model of the variable-speed FH signal can be given by

$$VSFH(t) = A(t) * \sum_n \text{rect}_{T_n}(t - \sum_{i=1}^{n-1} T_i - t_0) e^{j2\pi f_n(t - \sum_{i=1}^{n-1} T_i - t_0) + j\theta_n} * m(t) \quad (4)$$

where  $T_n$  denotes the dwell time at hop  $n$  and  $T_i$  denotes the dwell time at hop  $i$ .

### 2.2. Time–Frequency Analysis

The center frequency of FH signals exhibits irregular changes over time, which makes it difficult to comprehensively analyze FH signals in both the time and frequency domains. To effectively detect FH signals, it is common to utilize the time–frequency analysis techniques. The popular methods of time–frequency analysis mainly include STFT and Wigner–Ville distribution (WVD), as well as some relevant improved algorithms, and various joint time–frequency transforms.

For the received signal  $r(t)$ , the expression of STFT can be written as

$$\text{STFT}_r(t, f) = \int_{-\infty}^{+\infty} r(\tau) h^*(\tau - t) e^{-j2\pi f\tau} d\tau \quad (5)$$

where  $h(t)$  denotes the window function, and  $\tau$  denotes the delay time. According to (5), we can discover that STFT divides the received signal  $r(t)$  into multiple signal segments

which are processed by the window function, and then calculates the Fourier transform of each signal segment separately.

For the received signal  $r(t)$ , the expression of WVD can be written as

$$WVD_r(t, f) = \int_{-\infty}^{+\infty} r(t + \tau/2)r^*(t - \tau/2)e^{-j2\pi f\tau}d\tau \quad (6)$$

Considering the expression in (1), we can rewrite  $WVD_r(t, f)$  as

$$\begin{aligned} WVD_r(t, f) = & WVD_{FSFH}(t, f) + WVD_{VSFH}(t, f) + WVD_d(t, f) + WVD_c(t, f) \\ & + WVD_{FSFH,VSFH}(t, f) + WVD_{FSFH,d}(t, f) + WVD_{FSFH,c}(t, f) \\ & + WVD_{VSFH,d}(t, f) + WVD_{VSFH,c}(t, f) \\ & + WVD_{d,c}(t, f) \end{aligned} \quad (7)$$

where  $WVD_{FSFH}(t, f)$  is the WVD term of fixed-speed FH signal,  $WVD_{VSFH}(t, f)$  is the WVD term of variable-speed FH signal,  $WVD_d(t, f)$  is the WVD term of fixed-frequency interference signal,  $WVD_c(t, f)$  is the WVD term of sweep-frequency interference signal, and other terms are cross-terms between signal components.

Comparing the expression of STFT and WVD, it can be observed that cross-terms of different signal components will be generated during the transformation of WVD, making the fixed-speed FH signal and the variable-speed FH signal difficult to detect. Joint time–frequency transforms can suppress cross-terms and improve resolution, but the high computational complexity is not conducive to engineering implementation [27,28]. To avoid the cross-terms and reduce the computational complexity, we select STFT as the time–frequency analysis tool.

### 3. Algorithm Design

#### 3.1. Spectrogram Preprocessing

After STFT, the spectrogram of the received signal  $r(t)$  is obtained. Due to the presence of background noise and interference, it is hard to extract the FH signals directly. With the decline of SNR, the FH signals are easily submerged in the noisy background noise. To extract the FH signals from the spectrogram and reduce the impact of background noise and interference, we adopt the method of morphology filter to preprocess the spectrogram. The steps of preprocessing are as follows:

- (1) Select the rectangular structural element with length and width smaller than single hop to perform closed operation on the spectrogram to eliminate the impact of background noise and sweep-frequency interference.
- (2) Select the rectangular structural element with length slightly greater than the fracture area to perform the operation of corrosion on the spectrogram to complete the correlation and splicing of different signal fragments. Then, select the rectangular structural element with length slightly greater than the former rectangular structural element to perform the operation of expansion on the spectrogram for separating the aliasing regions in the spectrogram.
- (3) Utilize the method of OTSU to determine the binarization threshold. The method of OTSU divides the image data into two categories using a threshold. In one category, the grayscale of the pixels in the image is less than the threshold, while in the other category, the grayscale of the pixels in the image is greater than or equal to the threshold. When the variance of the grayscale between these two categories reaches the top, it indicates that the obtained threshold is the optimal threshold.

To obtain the optimal threshold, count the number of pixels for each grayscale in the image firstly. Set  $n_i$  as the number of pixels with grayscale  $i$  in the image,  $i = 0, 1, 2, \dots, 255$ . Thus, the probability of pixels with grayscale  $i$  in the image is given by

$$p_i = \frac{n_i}{\sum_{j=0}^{255} n_j} \quad (8)$$

Assume that all pixels in the image are divided into two categories, C1 and C2, with threshold  $k$ , and the probability of category C1 and C2 are written as  $p_1$  and  $p_2$ , respectively, and the average grayscale of category C1 and C2 are written as  $m_1$  and  $m_2$ , respectively.

$$p_1 = \sum_{i=0}^k p_i \quad (9)$$

$$p_2 = \sum_{i=k+1}^{255} p_i \quad (10)$$

$$m_1 = \frac{\sum_{i=0}^k i p_i}{p_1} \quad (11)$$

$$m_2 = \frac{\sum_{i=k+1}^{255} i p_i}{p_2} \quad (12)$$

Average grayscale of the entire image is given by

$$m_G = \sum_{i=0}^{255} i p_i \quad (13)$$

Combining with (9), (10), (11), and (12), we can update  $m_G$  as follows:

$$m_G = m_1 p_1 + m_2 p_2 \quad (14)$$

According to the definition of variance, the expression for intercategory variance is given by

$$\sigma^2 = p_1(m_1 - m_G)^2 + p_2(m_2 - m_G)^2 \quad (15)$$

Inserting (14) into (15), we can update  $\sigma^2$  as follows:

$$\sigma^2 = p_1 p_2 (m_1 - m_2)^2 \quad (16)$$

Traversing all grayscale levels  $[0, 254]$ , the  $k$  that maximizes  $\sigma^2$  is the optimal threshold.

- (4) Perform binarization segmentation to obtain the binary time–frequency image containing only FH signals and fixed–frequency interference signals based on the binarization threshold, with the signal grayscale of 1 and the background grayscale of 0.

### 3.2. Connected Domain Labeling

To remove fixed–frequency interference signals effectively, we adopt the method of connected domain labeling, which marks each white pixel in a binary image. The white pixels belonging to the same connected domain have the same mark, and the white pixels of different connected domains have different marks, so that each connected domain in the image can be extracted. In the method of connected domain labeling, there are two common connections: four–neighborhood connection and eight–neighborhood connection. To strengthen the correlation between adjacent regions, we adopt the pattern of eight–neighborhood connection. The steps of connected domain labeling are as follows:

- (1)  $label\_count = 1$ , and traverse each pixel of the binary time–frequency image in sequence (from left to right and from top to bottom).
- (2) If the pixel has already been traversed, continue traversing; otherwise, turn to step 3.
- (3) Set this pixel as the starting seed and place it in a set labeled as  $label\_count$ , then push all eligible pixels onto the stack based on the eight–neighborhood relationship.

- (4) Eject the top pixel of the stack and place it in the set labeled as  $label\_count$ , then push all eligible pixels onto the stack based on the eight-neighborhood relationship.
- (5) Repeat step 4 until the stack is empty,  $label\_count = label\_count + 1$ .
- (6) Repeat step 2 until the entire image is traversed.

### 3.3. Feature Extraction and Signal Sorting

After marking the connected domain of the binary time–frequency image, it is available to extract the feature. The method of feature extraction is to construct a minimum rectangular boundary for the connected domain, which can be represented by the vector  $(x, y, L, H)$ , where  $x$  and  $y$  denote the horizontal coordinates and the vertical coordinates of the left lower corner, respectively, and  $L$  and  $H$  denote the length of the x-axis and the y-axis, respectively.

Due to the constant frequency of the fixed-frequency interference signal, it is a straight line during the observation time in the spectrogram. The center frequency of the fixed-speed FH signal changes randomly over time, with some short horizontal lines of equal length on the spectrogram. Moreover, each hop of the fixed-speed FH signal is interconnected in time. Compared with the fixed-speed FH signal, each hop of the variable-speed FH signal has no fixed duration, with some short horizontal lines of different lengths on the spectrogram and each hop being interconnected in time. Based on the above analysis, we propose such a strategy of sorting: if the duration of each hop is equal to the observation time, regard the signal as fixed-frequency interference; if the duration of each hop is equal and is much less than the observation time, regard the signal as fixed-speed FH signal; if the duration of each hop is different and is much less than the observation time, regard the signal as variable-speed FH signal.

By analyzing the duration of each connected domain, we can easily find that the duration of each hop of FH signals and the duration of fixed-frequency interference signals are located in different high-density areas. Based on the feature, the DBSCAN (density-based spatial clustering of applications with noise) clustering algorithm is applied to distinguish between FH signals and fixed-frequency interference signals. The DBSCAN clustering algorithm is a classic density clustering algorithm that defines clusters as the largest set of points connected by density. This algorithm can divide regions with high density into clusters and find clusters of arbitrary shape in the noisy spatial database.

Compared with fixed-speed FH signal, the duration of each hop of the variable-speed FH signal has no regular distribution, causing DBSCAN clustering algorithm to be invalid. However, each hop of the variable-speed FH signal is interconnected in time, which means that the starting time of the next hop is equal to the ending time of the previous hop without considering channel-switching time. Based on the feature, we develop a time alignment algorithm, which is shown in Algorithm 1. According to the above analysis, we can know that the duration, the starting time, and the ending time are key parameters of each hop. We use the symbol  $t_d, t_s, t_e$  to represent the duration, the starting time, and the ending time, respectively,  $t_d = L, t_s = x, t_e = x + L$ , and input these three parameters into the parameter vector  $w = [t_s, t_e, t_d]$ .

In Algorithm 1, we sequentially traverse all components within the signal class and select different network signals by comparing the relationship between the end time of one component and the start time of other components. When the end time of a certain component is equal to the start time of another component, we consider these two components to be continuous in time and classify them into the same FH radio station. We repeat this cycle until the end time of a certain component is equal to the length of the observation time  $t_{observation}$ . Using Algorithm 1, we sequentially analyze the clustering results of the DBSCAN algorithm. Firstly, we utilize the time alignment algorithm for high-density clusters to separate the fixed-speed FH signals. This is because the high-density clusters include both all components of fixed-speed FH signals and certain components of variable-speed FH signals, and we use Algorithm 1 to identify all components belonging to the same fixed-speed FH radio station. After that, the remaining signal segments only

contain components of variable-speed FH signals. By using Algorithm 1 again, the sorting of variable-speed FH signals can be achieved.

**Algorithm 1:** The time alignment algorithm.

**Input:** the cluster of FH signal, the parameter vector of the first signal  $w_1$  in the cluster.

**Output:** sorting result  $\Phi_m$ .

```

1 Initialize:  $k = 2, m = 1, \Phi_m = w_1$ .
2 while  $\Phi_m \cdot w_m \cdot t_e < t_{observation}$  do
3   Extract the parameter vector of the  $k$ -th signal  $w_k$  in the cluster.
4   if  $w_k \cdot t_s = \Phi_m \cdot w_m \cdot t_e$  then
5      $m = m + 1$ .
6      $\Phi_m = [\Phi_{m-1}, w_k]$ .
7      $k = k + 1$ .
8   else
9      $k = k + 1$ .
10  end
11 end

```

To sum up, the sorting of a variable-speed FH signal is divided into two steps: (1) Utilize the time alignment algorithm for high-density clusters to separate the fixed-speed FH signal. (2) Utilize the time alignment algorithm for remaining signal segments to sort the variable-speed FH signal.

3.4. Algorithm Summary

We sort variable-speed FH signals from the perspective of image processing. Firstly, after performing STFT on the received signal, we adopt the methods of morphology filter and binary processing to filter out the background noise and sweep-frequency interference in the spectrogram. Secondly, we mark the white connected areas in the spectrogram for feature extraction. Thirdly, the starting time, the ending time, and the duration of each hop are obtained and the DBSCAN algorithm is applied to identify fixed-frequency interference based on these three characteristic parameters. Finally, the proposed algorithm about time alignment can detect and sort variable-speed FH signals from the remaining mixed FH signals. We summarize the proposed sorting algorithm about variable-speed FH signals in Figure 1.

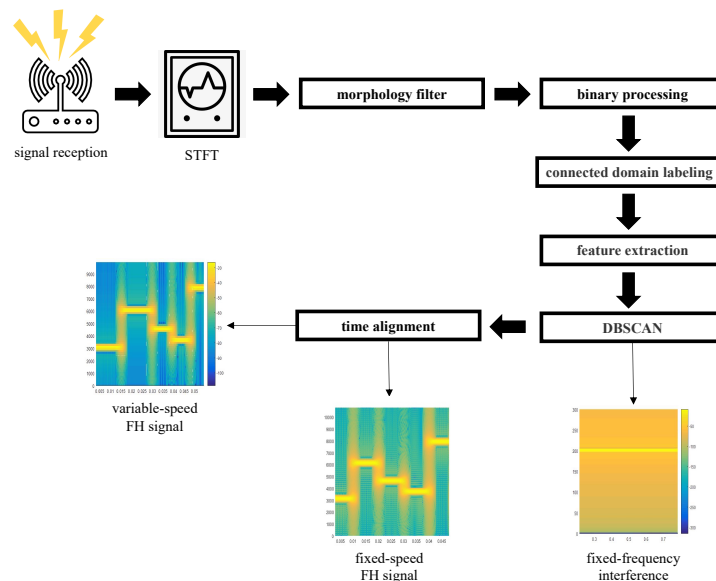


Figure 1. Flowchart of variable-speed FH signal sorting.

#### 4. Numerical Results

In this section, examples are provided to demonstrate the output result and sorting accuracy of the proposed algorithm. We consider the mixed signals containing white Gaussian noise, fixed-frequency interference signals, sweep-frequency interference signals, fixed-speed FH signals, and variable-speed FH signals, where the sampling rate of the mixed signals is 180 MHz and the sampling time is 2 s. The frequency set of fixed-frequency interference signals is [30, 50, 70, 90] MHz, the frequency range of sweep-frequency interference signal 1 is 20 MHz~40 MHz with the time length  $t_1 = 0.05$  s, the frequency range of sweep-frequency interference signal 2 is 30 MHz~50 MHz with the time length  $t_1 = 0.05$  s, and the SNR for white Gaussian noise is 0 dB. For fixed-speed FH signal 1, the frequency range is 30 MHz~50 MHz, the hopping speed is 100 hop/s, the modulation method is 2 FSK, and the symbol rate is 200 bit/s. For fixed-speed FH signal 2, the frequency range is 50 MHz~70 MHz, the hopping speed is 50 hop/s, the modulation method is 2 PSK, and the symbol rate is 100 bit/s. For variable-speed FH signals, the frequency range is 70 MHz~90 MHz, the range of hopping speed is 25 hop/s~100 hop/s, the modulation method is MSK, and the symbol rate is 50 bit/s. STFT adopts the Hamming window with the length of 1024 points.

##### 4.1. Morphology Filter and Binary Processing

We perform STFT transformation on the mixed signals to obtain the spectrogram. As shown in Figure 2, the spectrogram is filled with foggy noise, which is the form of white Gaussian noise after STFT. The fixed-speed FH signal is represented on the spectrogram as some short horizontal lines of equal length, and the variable-speed FH signal is represented on the spectrogram as some short horizontal lines of different lengths. The fixed-frequency signal is represented on the spectrogram as a continuous horizontal line, and the sweep-frequency signal is represented on the spectrogram as the short slash.

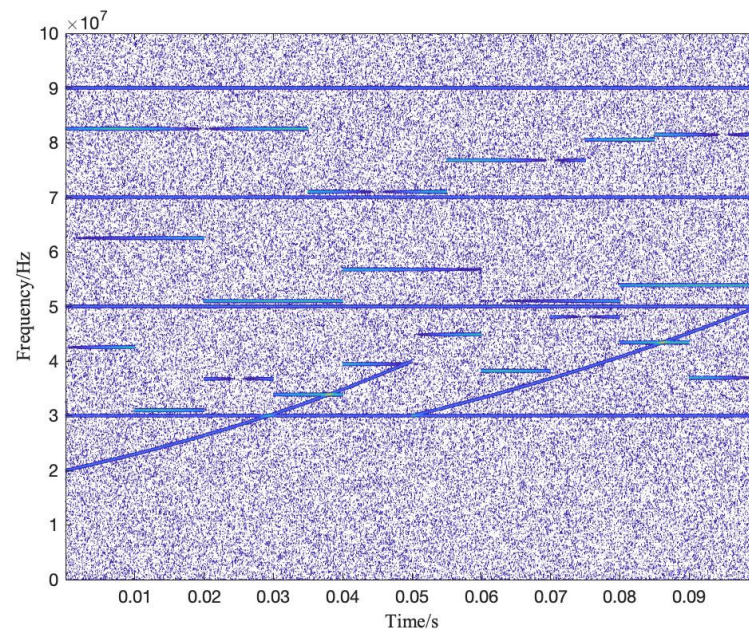


**Figure 2.** The original spectrogram (the observation time is 0.1 s).

To eliminate white Gaussian noise and sweep-frequency signal, we perform the operation of morphology filter on the spectrogram. As shown in Figure 3a, white Gaussian noise and sweep-frequency signal are filtered out. However, STFT can set the amplitude of some signal regions to 0, resulting in fractures in the connected areas of the same type of signal under low SNR conditions. Thus, it is necessary to associate the fracture fragments and then complete the stitching. The optimized spectrogram is shown in Figure 3b.

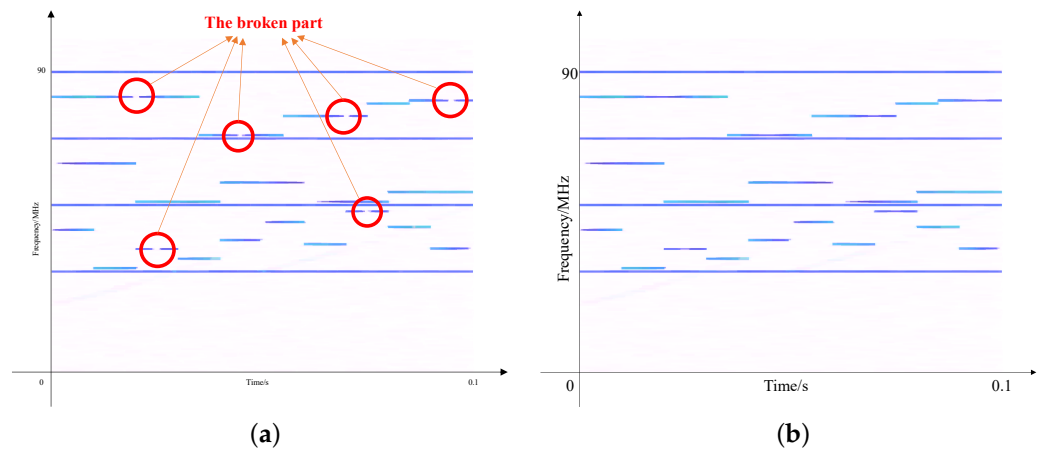


**Figure 3.** (a) The filtered spectrogram. (b) The optimized spectrogram.

Expanding the difference between signal and background is beneficial for connected domain labeling. We utilize the method of OTSU to determine the binarization threshold, and the binary processing of the optimized spectrogram is shown in Figure 4.

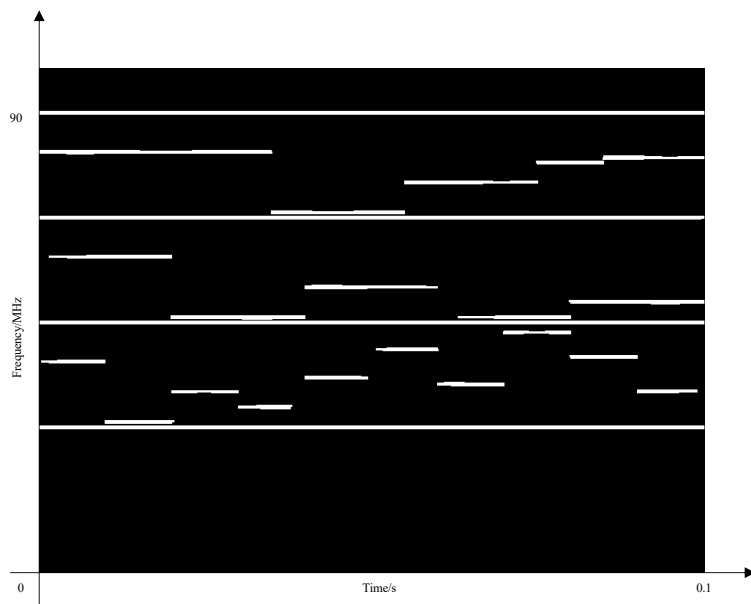


**Figure 4.** The binary processing of the optimized spectrogram.

#### 4.2. Connected Domain Labeling and Signal Sorting

It can be observed that the attributes of each connected region can effectively characterize the parameter characteristics of the signal from Figure 4. To extract these parameter characteristics, we label the connected regions, which are shown in Figure 5.

After labeling the connected domains, the parameter vector of each connected domain can be obtained. We extract the duration of each connected domain from the parameter vector and use the duration of each connected domain as a feature. The duration clustering based on the DBSCAN algorithm is performed on the connected domains, and the density parameter of sample distribution within the neighborhood is set to (30,1), which represents clustering with at least one point in a circular neighborhood with a radius of 30. The clustering result is shown in Figure 6, where labels [1,2,4,5] are category 1, label 3 is category 2, labels [6,8,10,11,14,15,17,19,20,22,24] are category 3, and labels [7,9,12,13,16,18,21,23] are category 4. Due to the duration of category 1 being equal to the observation time, labels [1,2,4,5] belong to fixed-frequency interference signal. The duration of categories [2,3,4] is

much shorter than the observation time, so categories [2,3,4] belong to FH signals, which include fixed-speed FH signals and variable-speed FH signals.

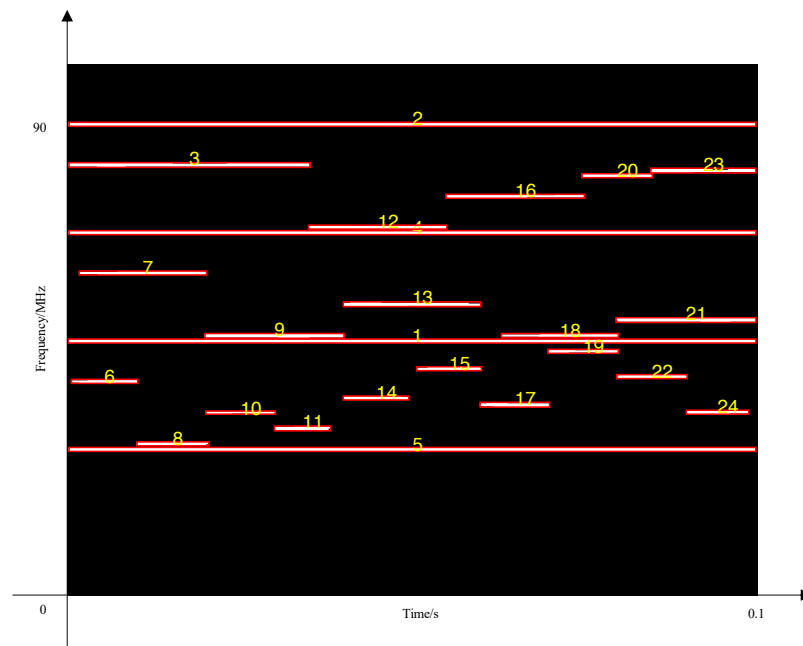


Figure 5. Connected domain after labeling.

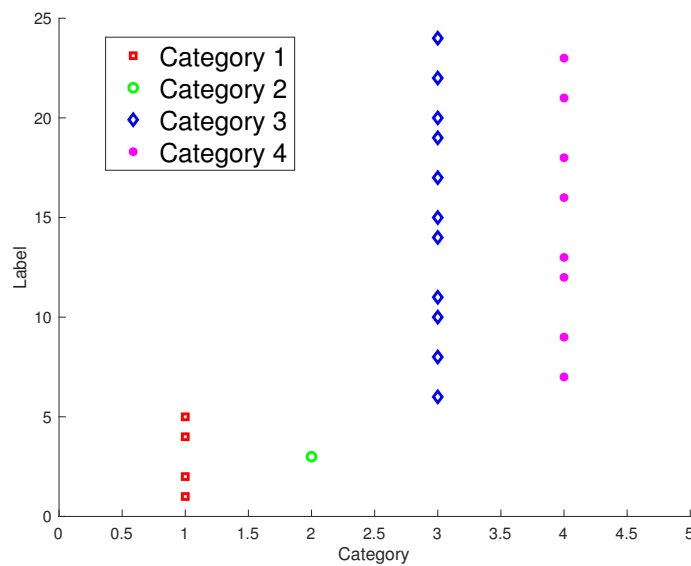


Figure 6. Clustering result.

The random duration of variable-speed FH signals makes it difficult to sort FH signals according to duration, and we adopt the proposed time alignment algorithm to solve this problem. Due to a large number of signal segments contained in category 3 and category 4, we think that category 3 and category 4 are high-density clusters and we input category 3 and category 4 into the time alignment algorithm to separate the fixed-speed FH signals. Then, we reuse the time alignment algorithm for the remaining signal segments. Figure 7 shows the result of signal sorting, where fixed-speed FH signal 1 is made up of labels [6,8,10,11,14,15,17,19,22,24], fixed-speed FH signal 2 is made up of labels [7,9,13,18,21], and the variable-speed FH signal is made up of labels [3,12,16,20,23].

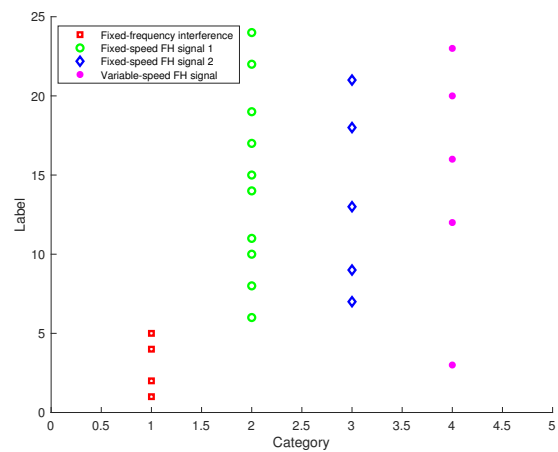


Figure 7. Sorting result.

#### 4.3. Testing in Code Division Networking

It can be seen from Figure 7 that the proposed algorithm is able to effectively sort variable-speed FH signals from multiple FH signals when the networking method of FH signals is frequency division networking (different FH signals use different frequency channels), and in this section, we test the output result of the proposed algorithm in the scene of code division networking (all FH signals work on the same frequency channel with different FH sequences, and the orthogonality of the FH sequences is used to distinguish different FH signals). The parameters are set as follows: For fixed-speed FH signal 1, the frequency range is 30 MHz~80 MHz, the hopping speed is 100 hop/s, the modulation method is 2FSK, and the symbol rate is 200 bit/s. For fixed-speed FH signal 2, the frequency range is 30 MHz~80 MHz, the hopping speed is 50 hop/s, the modulation method is 2 PSK, and the symbol rate is 100 bit/s. For variable-speed FH signal 1, the frequency range is 30 MHz~80 MHz, the range of hopping speed is 25 hop/s~100 hop/s, the modulation method is MSK, and the symbol rate is 50 bit/s. For variable-speed FH signal 2, the frequency range is 30 MHz~80 MHz, the range of hopping speed is 20 hop/s~100 hop/s, the modulation method is QPSK, and the symbol rate is 50 bit/s. In addition, there are white Gaussian noise ( $SNR = 0$  dB), fixed-frequency interference ( $f_1 = 58$  MHz,  $f_2 = 78$  MHz), and sweep-frequency interference (the frequency range  $f_r = 30$  MHz~50 MHz, the time length  $t_l = 0.025$  s) in the shortwave environment. The spectrogram is shown in Figure 8.

We input the spectrogram into the proposed algorithm, and the sorting process of the variable-speed frequency-hopping signal is shown in Figure 9. The output of the proposed algorithm indicates that the proposed algorithm can accurately sort mixed FH signals, which adopts the method of code division networking.

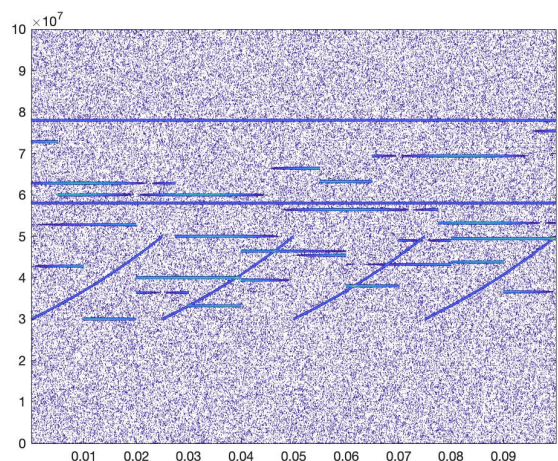


Figure 8. The original spectrogram.

#### 4.4. Comparison of Sorting Performance

In this section, we analyze the sorting performance of the proposed algorithm in different SNR conditions. The performance of the variable-speed FH signal sorting is evaluated using correct-sorting probability  $P_{cs}$ , which is defined in (17), and false alarm probability  $P_{fa}$ , which is defined in (18).

$$P_{cs} = \frac{\sum_{q=1}^Q \frac{b_q}{a}}{Q} \tag{17}$$

$$P_{fa} = \frac{\sum_{q=1}^Q \frac{c_q}{d}}{Q} \tag{18}$$

where  $Q = 1000$  is the number of independent trials,  $a$  is the actual number of variable-speed FH signal segments,  $b_q$  is the number of variable-speed FH signal segments sorted correctly with the sorting algorithm,  $c_q$  is the number of false variable-speed FH signal segments detected with the sorting algorithm, and  $d$  is the estimated number of variable-speed FH signal segments.

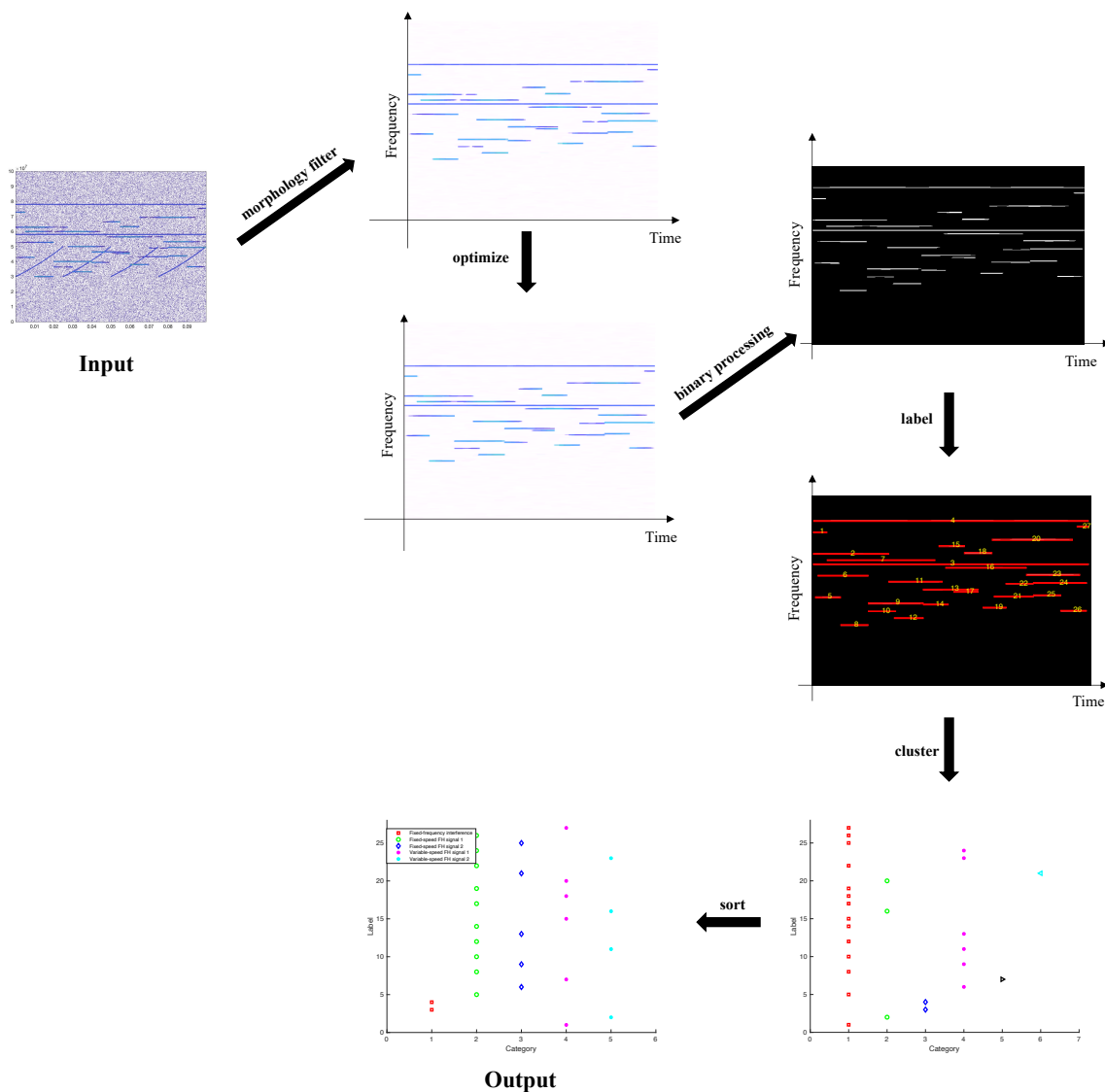


Figure 9. The sorting process of variable-speed frequency-hopping signals.

In Section 4.3, we set the number of category  $k = 5$  and we choose the algorithms in [29,30] as the compared algorithms. After STFT, filter operation, binary segmentation, connected domain labeling, and feature extraction, FH signal sorting is based on MeanShift algorithm in [29]. The MeanShift algorithm assumes that the datasets of different clusters conform to different probability density distributions. By finding the most dense direction in the sample set and constantly shifting to the maximum density, the samples converge to the local density maximum, and the points that converge to the same maximum are the members of the same cluster. In [30], FH signals sorting depends on K-means clustering, which implements the classification of the sample based on Euclidean distance between sample data and different centroids. Figure 10a compares the correct-sorting probability for the algorithms in [29,30] and the proposed algorithm, and Figure 10b compares the false alarm probability for the algorithms in [29,30] and the proposed algorithm.

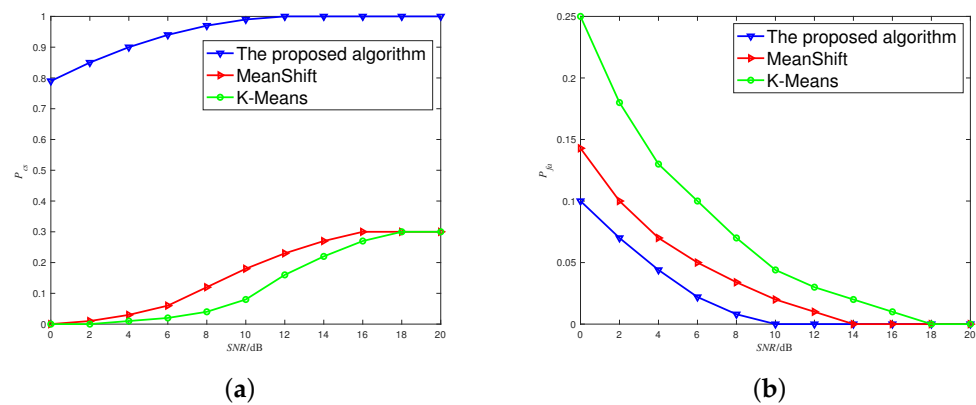


Figure 10. (a)  $P_{cs}$  versus SNR. (b)  $P_{fa}$  versus SNR.

As shown in Figure 10a, the sorting accuracy of the proposed algorithm is much higher than that of the algorithm in [29,30] in the same SNR conditions. Moreover, in high SNR conditions, the sorting accuracy of the proposed algorithm can reach 100%, while the sorting accuracy of the algorithm in the literature [29,30] can only reach 30%. There are two reasons for this difference:

(1) As shown in Figure 11a, the connected domain marked by the algorithm in [29,30] has some broken parts, causing the FH signal to be divided into multiple burst signals with shorter duration, which brings interference to subsequent clustering processing. Moreover, there are some overlaps of time and frequency dimensions in the time–frequency distribution, causing deformation of the connected domain, which brings significant errors to parameter extraction. In comparison, the connected domain marked by the proposed algorithm has no broken parts and overlaps, which can better reflect the time–frequency situation of the FH signal, as shown in Figure 11b.

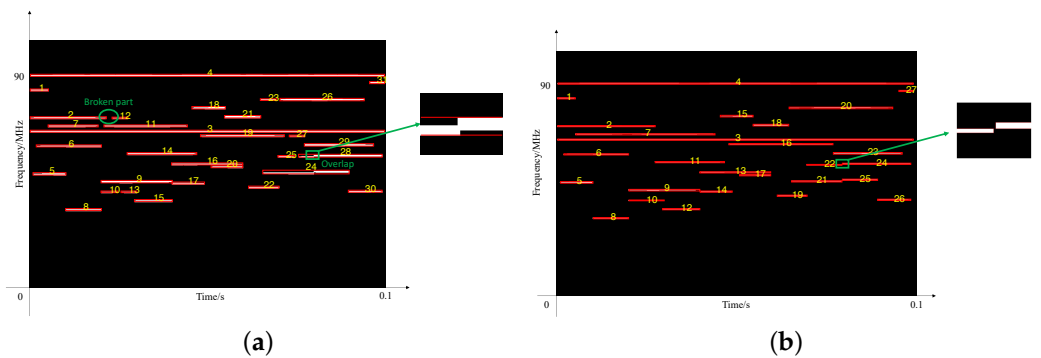
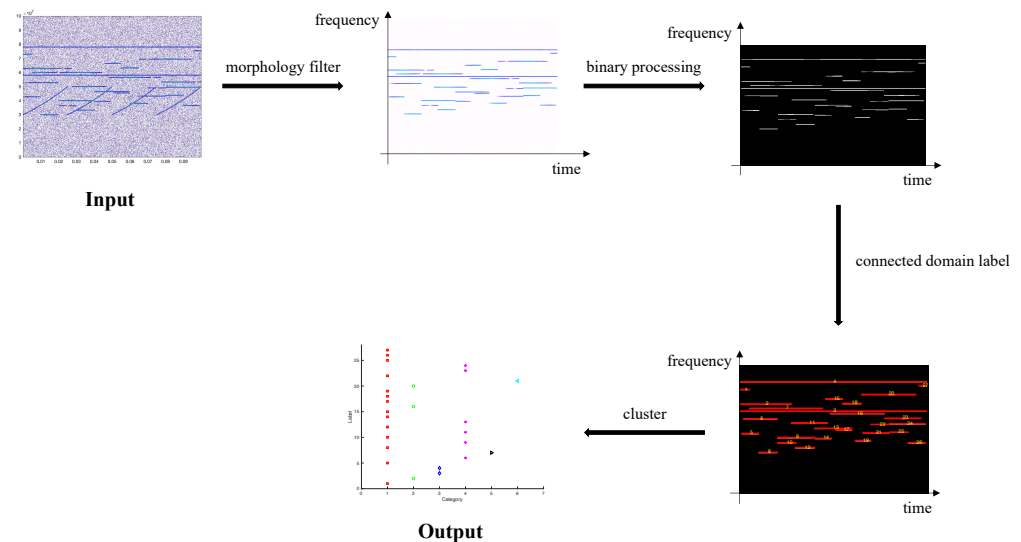


Figure 11. (a) Marked connected domain in [29,30]. (b) Marked connected domain in this paper.

(2) The proposed algorithm adopts the means of time alignment to sort multiple FH signals, which takes into account the random changes in duration and center frequency. However, the algorithm in [29,30] sorts multiple FH signals only based on their duration, which ignores the irregular distribution of the duration of variable-speed FH signals. The sorting process of variable-speed FH signals in [29,30] is shown in Figure 12.



**Figure 12.** The sorting process of variable-speed frequency-hopping signal in [29,30].

From Figure 12, it can be seen that the methods in [29,30] lack the optimization of time–frequency maps, resulting in some variable-speed FH signal segments being fragmented or overlapping with other signal segments. In addition, the methods in [29,30] do not consider the temporal continuity of FH signals, but simply classify them based on the duration of each hop signal, resulting in the inability to sort variable-speed FH signal segments which have the same duration as the fixed-speed FH signal segments. Therefore, whether under low SNR conditions or high SNR conditions, the sorting accuracy of the methods in [29,30] is far lower than that of the proposed algorithm.

As shown in Figure 10b, the false alarm probability of both the proposed algorithm and the comparison algorithm decreases with increasing SNR, with the proposed algorithm having the smallest false alarm probability, followed by the algorithm in [29], and the algorithm in [30] having the highest false alarm probability. This is because the proposed algorithm adopts the strategy of sorting fixed-speed FH signals first and then variable-speed FH signals, while the algorithm in [29,30] synchronizes the fixed-speed FH signals sorting with the variable-speed FH signals sorting, greatly increasing the false alarm probability.

In addition, we can see that the sum of correct-sorting probability and false alarm probability is not equal to 1; this is because the sorting of variable-speed FH signals is based on the detection of variable-speed FH signals. After detecting the variable-speed FH signal, it is necessary to group these variable-speed FH signal segments, and the same group of variable-speed FH signal segments indicates that these variable-speed FH signal segments come from the same FH radio station. During the grouping process, some variable-speed FH signal segments may entered the wrong group, resulting in a smaller number of correctly grouped variable-speed FH signal segments than the detected variable-speed FH signal segments. Therefore, the correct-sorting probability is lower than the detection probability. The correct-sorting probability describes the sorting situation of variable-speed FH signals, and the false alarm probability describes the detection situation of variable-speed FH signals. The sum of false alarm probability and detection probability is equal to 1. Combining the condition that the correct-sorting probability is less than the detection probability, it can be determined that the sum of correct-sorting probability and false alarm probability is less than 1.

## 5. Conclusions

A signal sorting method utilizing a spectrogram was proposed for variable-speed frequency-hopping (FH) signals. The objective was to mitigate the impact of interference signals and noise on FH signals and achieve blind detection and accurate sorting of variable-speed FH signals. In this method, the duration of the signal was utilized as the dataset for blind detection, enabling the separation of various interference signals and noise from the FH signals. Subsequently, a time alignment algorithm was employed to separate the fixed-speed FH signals from the mixed FH signals. Building upon this, the time alignment algorithm was reapplied to accurately sort the variable-speed FH signals from the remaining FH signals. The numerical results demonstrated that the proposed algorithm exhibited a high probability of correct sorting and a low false alarm probability, all without requiring any prior information. In comparison to alternative sorting algorithms for FH signals, the proposed method not only offered better representation of the time–frequency characteristics of the received signals but also achieved more accurate sorting of variable-speed FH signals.

**Author Contributions:** W.Z.: conceptualization, methodology, software, formal analysis, validation, writing—original draft, writing—review and editing; H.J.: conceptualization, formal analysis, writing—review and editing, supervision; J.W.: conceptualization, formal analysis, visualization, validation; Y.L.: conceptualization, methodology, supervision, project administration; C.L. (Caiyi Lou): conceptualization, resources, supervision, funding acquisition; C.L. (Changming Liu): conceptualization, investigation, resources, supervision. All authors have read and agreed to the published version of the manuscript.

**Funding:** This work was supported by the National Natural Science Foundation of China under grant number 62071479.

**Data Availability Statement:** Not applicable.

**Conflicts of Interest:** The authors declare no conflict of interest.

## References

1. Gu, C.; Wang, L. A Method for Orthogonal FH Signals Dynamic Sorting. *J. Astronaut.* **2012**, *33*, 1769–1776.
2. Aziz, J.S.; Al-Shalchi, A.A.; Al-Kateeb, A.K.; Pavlidou, F.N. Parameter Estimation of Frequency-Hopping (FH-SS) Signals Using Modified Autocorrelation Techniques. In Proceedings of the 2006 International Conference on Communication Technology, Guilin, China, 27–30 November 2006; pp. 1–4. [\[CrossRef\]](#)
3. Gao, P.; Hu, S.; Wu, Y. A Shortwave Signal Detection Algorithm Based on Spectrum Energy Statistics. *Digit. Technol. Appl.* **2013**, *10*, 124–125.
4. Bu, G.; Luo, M. Frequency Measurement Study of Frequency Hopping Signal Based on Digital Channelization. *Shipboard Electron. Countermeas.* **2015**, *38*, 62–64.
5. Zhang, D.; Guo, Y.; Huo, W.; Fan, C.Z.; Zhang, B. An Improved Channelized Detection Method of Frequency Hopping Signals. *Fire Control Command Control* **2012**, *37*, 58–61.
6. Lv, L.; Yi, Y.; Lu, Y. Detection of Shortwave Frequency Hopping Signal Based on Overlapped-Sliding Time-Frequency Analysis. *Electron. Inf. Warf. Technol.* **2020**, *35*, 25–29.
7. Li, S.; Li, T. Frequency Hopping Signal Detection over The Shortwave Channel. *Acta Electron. Sin.* **2019**, *47*, 623–629.
8. Zhang, S.; Yao, Z.; Fan, Z.; Wang, H.Y.; Wu, Z.H. Frequency Hopping Signal Extraction and Detection Based on Local Adaptive Threshold. *Electron. Opt. Control* **2020**, *27*, 68–72.
9. Hou, F.; Yao, Z.; Yang, J.; Li, Y.; Wang, Z. A Fast Detection Method of Frequency Hopping Signal Based on K-Means Clustering. *Telecommun. Eng.* **2022**, *62*, 199–205.
10. Ye, J.; Zou, J.; Gao, J.; Zhang, G.; Kong, M.; Pei, Z.; Cui, K. A New Frequency Hopping Signal Detection of Civil UAV Based on Improved K-Means Clustering Algorithm. *IEEE Access* **2021**, *9*, 53190–53204. [\[CrossRef\]](#)
11. Qu, Y.; Pei, Y.; Song, D. Frequency-Hopping Signal Sorting Based on Deep Learning. In Proceedings of the 2019 IEEE 2nd International Conference on Electronic Information and Communication Technology (ICEICT), Harbin, China, 20–22 January 2019; pp. 759–762. [\[CrossRef\]](#)
12. Wang, Z.; Zhang, B.; Zhu, Z.; Wang, Z.; Gong, K. Signal Sorting Algorithm of Hybrid Frequency Hopping Network Station Based on Neural Network. *IEEE Access* **2021**, *9*, 35924–35931. [\[CrossRef\]](#)
13. Lee, K.G.; Oh, S.J. Detection of Frequency-Hopping Signals with Deep Learning. *IEEE Commun. Lett.* **2020**, *24*, 1042–1046. [\[CrossRef\]](#)

14. Deng, Z.; Lei, J.; Sun, C. Semi-Supervised Interference Cancellation Method for Frequency Hopping Signal Blind Detection. *Syst. Eng. Electron.* **2022**, *in press*.
15. Dong, R.; Guo, Y.; Yu, X. A Frequency Hopping Signal Detection Method Based on Sparse Reconstruction. *J. Air Force Eng. Univ. (Nat. Sci. Ed.)* **2018**, *19*, 77–82.
16. Xu, M.; Ping, X.; Li, T.; Xu, M. A New Time-Frequency Spectrogram Analysis of FH Signals by Image Enhancement and Mathematical Morphology. In Proceedings of the Fourth International Conference on Image and Graphics (ICIG), Chengdu, China, 22–24 August 2007; pp. 610–615.
17. Luo, S.; Luo, L. Adaptive Detection of An Unknown FH Signal Based on Image Features. In Proceedings of the 2009 5th International Conference on Wireless Communications, Networking and Mobile Computing, Beijing, China, 24–26 September 2009.
18. Wang, M.; Gong, X.; Luo, R.; Bian, T.; Wang, Z. Joint Blind Parameter Estimation of Frequency Hopping Signal Based on Adaptive Morphology. *Syst. Eng. Electron.* **2021**, *43*, 1398–1405.
19. Yan, J.; Liang, T.; Qi, Z. Research on the Frequency Hopping Communication Technology of Variable Hopping Rate and Variable Interval. *Wirel. Commun. Technol.* **2012**, *4*, 25–29.
20. Yu, X.; Guo, Y.; Zhang, K. A Network Sorting Algorithm Based on Blind Source Separation of Multi-FH Signal. *Signal Process.* **2017**, *33*, 1082–1089.
21. Li, H.; Guo, Y.; Zhang, D.; Yang, Y.; Qi, Z.; Sui, P. Synchronous Frequency Hopping Signal Network Station Sorting Based on Underdetermined Blind Source Separation. *J. Electron. Inf. Technol.* **2021**, *43*, 319–328.
22. Wang, M.; Cai, X.; Lei, Y. Variable Speed Hopping Signal Sorting Algorithm Based on Frame Overlap. *J. Detect. Control* **2020**, *42*, 63–68.
23. Yang, B.; Chen, Y.; Luan, Y.; Liu, J. A Blind Separating Method for Asynchronous Nonorthogonal Frequency Hopping Network. *High Power Laser Part. Beams* **2015**, *27*, 264–269.
24. Tang, N.; Guo, Y.; Zhang, K. A Sorting Method for Underdetermined Frequency Hopping Networks Based on SCA. *Syst. Eng. Electron.* **2017**, *39*, 2817–2823.
25. Hou, F.; Yao, Z.; Yang, J. A Blind Source Separation Algorithm for Multi-Frequency Hopping Signals Based on Time-Frequency Analysis. *Ordnance Ind. Autom.* **2022**, *41*, 15–19.
26. Fu, W.; Zhang, Y.; Wei, J. Blind Parameter Estimation Algorithm for Frequency-Hopping Signals Based on Compressed Sensing. *J. Commun.* **2017**, *38*, 48–56.
27. Wang, L.; Zhan, H.; Chen, S. Joint Algorithm for Blind Estimation of FH Signal Based on STFT and PWVD. In Proceedings of the 2021 IEEE 5th Advanced Information Technology, Electronic and Automation Control Conference (IAEAC), Chongqing, China, 12–14 March 2021; pp. 1413–1417. [[CrossRef](#)]
28. Zhang, D.; Shang, Y.; Liang, X.; Wang, L.; Yin, C. Joint Blind Estimation of Multidomain Parameters for Multiple Frequency Hopping Signals. In Proceedings of the 2022 IEEE 5th International Conference on Automation, Electronics and Electrical Engineering (AUTEEE), Shenyang, China, 18–20 November 2022; pp. 657–665. [[CrossRef](#)]
29. Zhu, Z.; Lin, Y.; Wang, Z.; Gong, K.; Chen, P.; Wang, Z.; Liang, J. Fast Blind Detection of Shortwave Frequency Hopping Signal Based on MeanShift. *J. Commun.* **2022**, *43*, 200–210. [[CrossRef](#)]
30. Li, H.; Guo, Y.; Qi, Z. Blind Detection of Multi-Frequency Hopping Signals under Complex Electromagnetic Environment. *J. Huazhong Univ. Sci. Technol. (Nat. Sci. Ed.)* **2020**, *48*, 13–19. [[CrossRef](#)]

**Disclaimer/Publisher’s Note:** The statements, opinions and data contained in all publications are solely those of the individual author(s) and contributor(s) and not of MDPI and/or the editor(s). MDPI and/or the editor(s) disclaim responsibility for any injury to people or property resulting from any ideas, methods, instructions or products referred to in the content.